

## Parameterization of dispersion in two-dimensional turbulence

By C. PASQUERO<sup>1,2</sup>, A. PROVENZALE<sup>2</sup> AND A. BABIANO<sup>3</sup>

<sup>1</sup>Doctorate Program in Fluid Dynamics, Politecnico di Torino, Italy

<sup>2</sup>Istituto di Cosmogeofisica, CNR, Torino, Italy

<sup>3</sup>Laboratoire de Météorologie Dynamique, ENS, Paris, France

(Received 19 September 2000 and in revised form 28 December 2000)

We investigate the performance of standard stochastic models of single-particle dispersion in two-dimensional turbulence. Owing to the presence of coherent vortices, particle dispersion in two-dimensional turbulence is characterized by a non-Gaussian velocity distribution and a non-exponential velocity autocorrelation, and it cannot be properly captured by either linear or nonlinear stochastic models with a single component process. Based on physical and dynamical considerations, we introduce a family of two-process stochastic models that provide a better parameterization of turbulent dispersion in rotating barotropic flows.

---

### 1. Introduction

A classic approach to the study of tracer advection is based on separating the ‘mean flow’ (that is slowly variable in space and time) from the turbulent dynamics acting on smaller scales, provided that the scale separation between the two components is large enough. The advective velocity is then given by the sum of a large-scale component  $U(\mathbf{x}, t)$  and of a turbulent velocity  $\mathbf{u}(\mathbf{x}, t)$ . Here,  $t$  is time and  $\mathbf{x}$  is the spatial position. In several instances, the large-scale part  $U(\mathbf{x}, t)$  can be modelled as a deterministic velocity field representing e.g. an oceanic jet (Samelson 1992; Poje & Haller 1999), a train of waves (Weiss & Knobloch 1987; Pierrehumbert 1991), or the coarse-grained general circulation of the atmosphere (Pierrehumbert & Yang 1993; von Hardenberg *et al.* 2000). In such an approach, studies employing the methods of chaotic advection naturally ensue (e.g. Samelson 1992; Wiggins 1992; Rogerson *et al.* 1999; Haller & Yuan 2000).

Deeper difficulties arise when dealing with the representation of the turbulent component  $\mathbf{u}(\mathbf{x}, t)$ . In several applications to tracer dispersion in the atmospheric boundary layer and in large- and mesoscale ocean flows, the turbulent velocity  $\mathbf{u}$  is taken as a random variable. The characteristics of the stochastic process describing its evolution are determined by the observed Lagrangian statistical properties (see e.g. Gifford 1982; Thomson 1987; Griffa 1996). For an extensive review on Lagrangian stochastic models of turbulent diffusion, see e.g. Rodean (1996).

In the limit of a continuous tracer distribution,  $c(\mathbf{x}, t)$ , the above approach leads to the formulation of an advection–diffusion equation where the large-scale velocity is responsible for the advection term and the turbulent velocity generates the diffusive behaviour on small scales. In the simplest formulation, the effect of the turbulent velocity is parameterized in terms of a Fickian diffusion term,  $\nabla \cdot (\kappa \cdot \nabla c)$ , sometimes

called ‘eddy diffusion’. The tensorial diffusion coefficient  $\kappa$  can vary in space and time and it is determined by the local properties of the turbulent velocity.

In most geophysical flows, however, the presence of coherent structures, be they convective plumes or long-lived vortices, complicates the picture depicted above and leads to tracer dispersion properties that cannot be properly captured by simple advection–diffusion models. In the case of the ocean, the work of Figueroa & Olson (1994) on tracer dispersion in a wind-driven double gyre has shown that advection–diffusion with a spatially variable diffusion coefficient cannot satisfactorily represent the dynamics of advected tracers in the presence of energetic mesoscale eddies. Analogously, the analysis of the trajectories of sub-surface ocean floats (Bracco, LaCasce & Provenzale 2000*a*), the results of laboratory experiments (Solomon, Weeks & Swinney 1993), and the numerical exploration of the dynamics of two-dimensional turbulence (Min, Mezić & Leonard 1996; Jiménez 1996; Weiss, Provenzale & McWilliams 1998; Bracco *et al.* 2000*b*) have shown that the turbulent velocities, the velocity gradients, and the particle displacements display a non-Gaussian distribution whenever strong coherent vortices are present.

Building upon these considerations, here we explore the performance of standard stochastic parameterizations when applied to systems where coherent vortices play a significant role, and study the dispersion of passive tracers in two-dimensional turbulence. We then use the approach discussed by Thomson (1987) and introduce a nonlinear stochastic process that produces the observed velocity p.d.f. A further improvement is based on introducing a stochastic model with two component processes, that allow a physically based, albeit slightly more complicated, stochastic parameterization of dispersion in vortex-dominated flows to be defined.

The rest of the paper is organized as follows. In §2 we discuss the basic properties of two-dimensional turbulence and the numerical scheme that we adopt to solve the equations. In §3 we discuss the Lagrangian statistical properties of two-dimensional turbulence. In §4 we discuss the performance of standard linear and nonlinear stochastic models, and we compare their predictions with the results obtained from the turbulence integration. In §5, the discrepancies between the properties of the standard stochastic models and those of turbulence motivate the introduction of a two-component stochastic model that accounts for the effect of coherent structures on tracer dispersion. Finally, §6 gives conclusions and perspectives. We relegate to the Appendix all technical details on the stochastic models introduced in §§4 and 5.

## 2. Dynamics of two-dimensional turbulence

The equation of motion of two-dimensional turbulence can be written as (see e.g. Pedlosky 1987; Salmon 1998)

$$\frac{D\omega}{Dt} = \frac{\partial\omega}{\partial t} + [\psi, \omega] = f + d \quad (2.1)$$

where  $\psi$  is the stream function,  $\omega = \nabla^2\psi$  is vorticity,  $D/Dt = \partial/\partial t + [\psi, \cdot]$  is the total advective derivative,  $[\cdot, \cdot]$  is the Jacobian operator, and  $f$  and  $d$  represent forcing and dissipation respectively. When the right-hand side of equation (2.1) vanishes, both the total kinetic energy

$$E = \frac{1}{2} \int (\nabla\psi)^2 dx dy$$

---


$$l_c = 0.013; \quad l_d = \pi; \quad t_c = 3.4 \times 10^{-5}; \quad t_d = 0.14; \quad \mathbf{k}_F = (0, 40)$$

$$\text{Resolution} = 512 \times 512 \text{ grid points.}$$


---

TABLE 1. Values of the parameters used in the simulation of two-dimensional turbulence discussed in the text.

---

and the total enstrophy

$$Z = \frac{1}{2} \int (\nabla^2 \psi)^2 dx dy$$

are conserved. The simultaneous conservation of these two quantities leads to a direct (from large to small scales) cascade of enstrophy and an inverse (from small to large scales) cascade of energy, that are associated with the formation of coherent structures (McWilliams 1984). In this study, both forcing and dissipation differ from zero, but, as previously shown (see e.g. Babiano *et al.* 1987a; Legras, Santangelo & Benzi 1988), vortices form as well.

In the simulations considered here, two energy sinks are introduced: one accounts for dissipation by viscous forces acting on small scales, while the other acts mostly on large scales as a friction term, preventing energy accumulation due to the inverse energy cascade. The total dissipation is given by

$$d = -t_c^{-1}(-l_c^2 \nabla^2)^8 \omega + t_d^{-1} l_d^{-2} \psi$$

where  $t_c$  and  $t_d$  are characteristic times,  $l_c$  is the lower cutoff scale and  $l_d$  is the largest scale. The iterated Laplacian represents a *hyper-viscosity* (Basdevant & Sadourny 1983), and it effectively dissipates enstrophy near the cutoff scale  $l_c$ , while the term proportional to the stream function  $\psi$  dissipates energy and enstrophy mostly at large scales.

The forcing acts at a given wavenumber  $\mathbf{k}_F$ , where energy and enstrophy are injected into the system. This is achieved by forcing the enstrophy spectrum to keep a constant value at the forcing wavenumber  $\mathbf{k}_F$ , while the phase is allowed to evolve freely. In other words,

$$|\hat{\omega}(\mathbf{k}_F)| = F$$

where  $\hat{\omega}$  is the Fourier transform of vorticity.

To have a statistically stationary field, the values of the parameters in the dissipation and forcing terms are chosen such that the total energy and enstrophy are approximately constant. In order to emphasize the intrinsic nonlinear dynamics of the system (represented by the Jacobian term in (2.1)), forcing and dissipation are kept as low as possible. The parameter values used in the simulation are listed in table 1. Equation (2.1) is integrated in a doubly periodic square domain, with size  $L \times L$ , where  $L = 2\pi$ . Details on the numerics can be found in Elhmaidi, Provenzale & Babiano (1993). A snapshot of the vorticity field, after statistical stationarity has been achieved, is shown in figure 1.

The mean enstrophy is  $\bar{Z} = Z/L^2 \sim 1.3 \times 10^5$  and the mean energy is  $\bar{E} = E/L^2 \sim 650$ . The flow has been integrated for a total time  $T = 0.763$ , corresponding to about 275 eddy turnover times  $T_Z$ , where  $T_Z = \bar{Z}^{-1/2} \sim 0.0028$ . During the integration, the enstrophy varies by about 3% around its mean value and the energy varies by up to 5%.

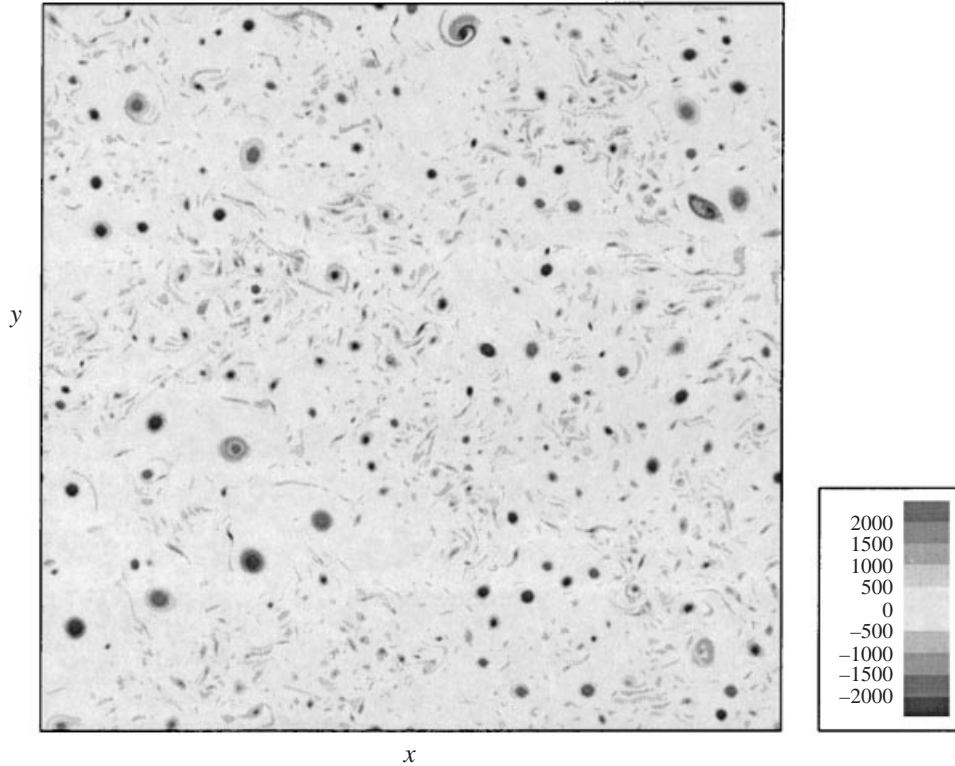


FIGURE 1. A snapshot of the vorticity field obtained by integration of the two-dimensional turbulence equation (2.1) with the parameters listed in table 1.

### 3. Lagrangian properties of two-dimensional turbulence

To determine the Lagrangian properties of two-dimensional turbulence, we introduce an ensemble of passively advected tracers in the time-evolving turbulent flow, discussed in §2. The particles are assumed not to affect the dynamics of the fluid, to be neutrally buoyant and to have infinitesimally small size, so that inertial effects can be discarded (see e.g. Maxey & Riley 1983 and Michaelides 1998 for a discussion of the dynamics of particles with finite size and non-vanishing inertia).

In the present case, the Lagrangian velocity of a particle is given by the Eulerian velocity at the particle location. The equations of motion become

$$\left. \begin{aligned} \dot{X}_i &= u(X_i, Y_i, t), \\ \dot{Y}_i &= v(X_i, Y_i, t), \end{aligned} \right\} \quad i = 1, \dots, M,$$

where  $X_i = (X_i, Y_i)$  and  $t$  are the spatial and temporal coordinates of the  $i$ th tracer particle and  $M$  is the total number of particles. (From now on, lower case letters,  $x$  and  $u$ , indicate Eulerian quantities and upper case letters,  $X$  and  $U$ , indicate Lagrangian quantities.) In a divergenceless field, the velocity is expressed as

$$u(X, Y, t) = - \left( \frac{\partial \psi}{\partial y} \right)_{X,Y,t}, \quad v(X, Y, t) = \left( \frac{\partial \psi}{\partial x} \right)_{X,Y,t}.$$

Numerically, the Lagrangian trajectories are integrated with a leapfrog scheme. A



FIGURE 2. Sample trajectories of Lagrangian tracers in two-dimensional turbulence.

third-order cubic spline interpolation of the Eulerian velocity field is used to compute the velocity at the particle positions.

A total set of  $M = 16\,384$  tracers is randomly seeded in the turbulent field once statistical stationarity is achieved. A few example trajectories are shown in figure 2. The sampling time is  $\delta t = 0.001T_Z \sim 0.36T_Z$ , and each trajectory is composed of  $N = 763$  data points.

Owing to the strong vorticity gradients at their edges, vortices act as transport barriers (see e.g. Elhmaidi *et al.* 1993; Babiano *et al.* 1994; Provenzale 1999). This means that tracers can enter a vortex only during its formation phase, and can exit from it mainly during vortex merging and filamentation. Particles can thus be trapped in vortices for long periods of time, and their motion is characterized by a fast rotation inside the vortex and a longer-term displacement due to the motion of the vortex itself (see e.g. the bottom trajectory in figure 2). Notice that the average displacement of an individual vortex in a system of many vortices is not significantly different from that of a particle in the background (Weiss *et al.* 1998). Therefore, in two-dimensional turbulence, the dynamics of a trapped particle is, on scales larger than the size of the vortex, statistically similar to that of any other particle.† For this reason, we do not separate tracers according to their position with respect to the Eulerian flow characteristics. Rather, we aim at determining the average dispersion

† A different situation may be encountered on the  $\beta$ -plane or for equivalent barotropic turbulence, where the vortices and the background can have different dynamics.

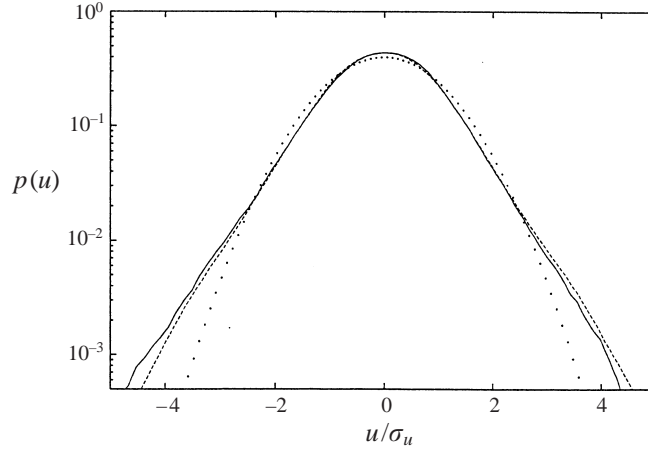


FIGURE 3. Normalized velocity p.d.f.s for the Eulerian field (solid line) and for the Lagrangian trajectories (dashed line). The dotted line represents a Gaussian distribution with the same variance as the observed p.d.f.s.

properties of this system, without resolving the fast rotational component of tracers trapped in vortices.

### 3.1. Velocity distribution

The average kinetic energy of Lagrangian trajectories is defined as

$$E_L = \frac{1}{2T} \int_0^T \langle U_i^2(t) + V_i^2(t) \rangle dt$$

where  $\mathbf{U}_i = (U_i, V_i)$  is the Lagrangian velocity of the  $i$ th particle, the angular brackets indicate an average over the whole set of tracers,  $\langle \cdot \rangle = (1/M) \sum_{i=1}^M \cdot$ , and  $T$  is the integration time. The mean Lagrangian kinetic energy is  $E_L \sim \bar{E} \sim 650$  (i.e. approximately equal to the mean Eulerian kinetic energy), confirming that the tracer trajectories considered here span the whole domain and provide a good sampling of the different regions. This indication is confirmed by the probability density functions (p.d.f.s) of the velocity components  $u$  and  $v$ . When calculating the velocity p.d.f.s for either the set of Lagrangian tracers or the Eulerian field, no significant difference between the two is found, as shown in figure 3. A chi-square test has been performed, indicating that the Eulerian and Lagrangian p.d.f.s can be considered to be drawn from the same distribution with a confidence larger than 99.9%. Notice that  $u$  and  $v$  have been considered together, owing to the isotropy of the field.

Figure 3 indicates that the velocity p.d.f.s in the forced turbulent field considered here are non-Gaussian. Previous studies have already discussed the shape of the velocity p.d.f. in freely decaying two-dimensional turbulence, revealing that the presence of coherent vortices leads to a non-Gaussian velocity distribution (Jiménez 1996; Min *et al.* 1996; Weiss *et al.* 1998; Bracco *et al.* 2000b). As shown by Bracco *et al.* (2000b), the non-Gaussianity that appears at high Reynolds numbers is entirely generated by the far field induced by the vortices. By contrast, the velocity p.d.f. associated with the background vorticity is Gaussian. This characteristic is observed for both freely decaying turbulence ( $f = 0$ ) and for forced turbulence, provided the Reynolds number is high enough and the forcing acts on small scales, as in the present case. By contrast, two-dimensional turbulence forced at large scales and at moderate Reynolds number

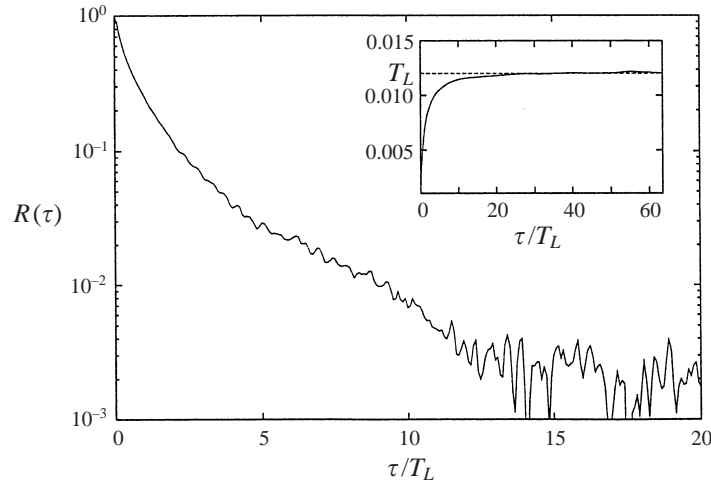


FIGURE 4. Lagrangian velocity autocorrelation,  $R(\tau)$ , as obtained from the dynamics of passively advected tracers in two-dimensional turbulence. In the inset, we show the integral  $\int_0^\tau R(\rho) d\rho$ ; the value reached at the plateau at large times provides an estimate of the Lagrangian decorrelation time  $T_L$ .

leads to larger and smoother vortices and consequently to Gaussian velocity p.d.f.s (Provenzale, Babiano & Villone 1995). Thus, also in the case of forced turbulence the properties of the velocity p.d.f.s are determined by the shape and the size of the vortices. In turn, these latter depend on the Reynolds number and the forcing scale.

### 3.2. Temporal correlations

The Lagrangian autocorrelation function  $R(t_0, \tau)$  is defined as

$$R(t_0, \tau) = \frac{\langle \mathbf{U}_i(t_0 + \tau) \cdot \mathbf{U}_i(t_0) \rangle}{(\langle \mathbf{U}_i(t_0 + \tau)^2 \rangle \cdot \langle \mathbf{U}_i(t_0)^2 \rangle)^{1/2}}.$$

Since the velocity field is statistically stationary, this function does not depend on the particular time  $t_0$  chosen for its computation. The explicit dependence on  $t_0$  can thus be removed by a further average over several (uncorrelated) values.

The autocorrelation function  $R(\tau)$  for the two-dimensional turbulent field considered above is shown in figure 4. From this function, the Lagrangian decorrelation time  $T_L$  is defined as

$$T_L = \int_0^\infty R(\rho) d\rho.$$

This gives  $T_L \sim 0.012 \sim 4.3T_Z$ . From now on, time will be expressed in units of the Lagrangian integral time  $T_L$ . Notice, also, that  $R(\tau)$  does not have an exponential shape. We shall discuss this point further in §5.

### 3.3. Single-particle dispersion

To further characterize the Lagrangian dynamics, we consider the statistics of the tracer displacements during a time  $\tau$ , i.e.

$$\Delta \mathbf{X}_i(t_0, \tau) = \mathbf{X}_i(t_0 + \tau) - \mathbf{X}_i(t_0).$$

Again, statistical stationarity allows the dependence on  $t_0$  to be removed, by averaging over several values. The second-order moment of the distribution of the tracer

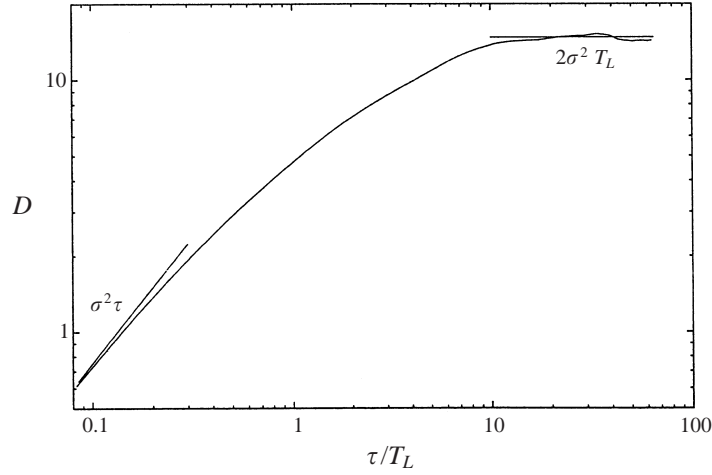


FIGURE 5. Dispersion coefficient,  $D(\tau)$ , as a function of time. The two straight lines represent the two asymptotic laws  $D \propto \tau$ , corresponding to ballistic motion at small times, and  $D \approx \text{const}$  for the Brownian regime at large times. Time is expressed in units of the Lagrangian decorrelation time,  $T_L$ .

displacements provides an estimate of the (time-dependent) dispersion coefficient  $D(\tau)$ , here defined as

$$D(\tau) = \frac{\langle |\Delta \mathbf{X}_i(\tau)|^2 \rangle}{2\tau}.$$

As shown by Taylor (1921),  $D(\tau) \propto \tau$  for  $\tau \rightarrow 0$  (the ballistic regime), and  $D(\tau) \rightarrow \text{const}$  for  $\tau \rightarrow \infty$  (the Brownian regime).

Figure 5 shows  $D(\tau)$  for the two-dimensional turbulent field investigated here. At very small values of  $\tau$ , the dispersion coefficient grows linearly in time.  $D(\tau)$  continues to grow, albeit more slowly, for values of  $\tau$  smaller than a few Lagrangian decorrelation times. For  $\tau \gtrsim 10T_L$ , the dispersion coefficient saturates on average, indicating that the Brownian regime is reached. Fluctuations of about 5% around the mean saturation value are due to variations in the energy of the advecting field and to limited statistics at large times. The higher-order moments of the distribution of displacements indicate significant deviations from Gaussianity at small times,  $\tau \ll T_L$ , as shown in figure 6. At times of the order of  $2T_L$ , the kurtosis,  $k = \langle \Delta X^4 \rangle / \langle \Delta X^2 \rangle^2$ , becomes very close to the Gaussian value  $k_g = 3$  (see figure 6c).

Finally, we define the first exit time  $T_{f,i}(t_0, r)$  for a given Lagrangian tracer as the minimum time it takes to reach a distance  $r$  from the position at time  $t_0$ , i.e. the minimum time  $T_{f,i}$  for which

$$|\Delta \mathbf{X}_i(t_0, T_{f,i})| = r.$$

The mean first exit time  $T_f(r)$  for two dimensional turbulence, as obtained by averaging over all tracers and over  $t_0$ , is shown in figure 7. The upper and lower lines include 95% of the values of  $T_{f,i}$  as computed from the individual particle trajectories.

We now have significant information on the bulk Lagrangian statistical properties of two-dimensional turbulence, which can be used to test the validity of stochastic models devised to parameterize turbulent particle dispersion.



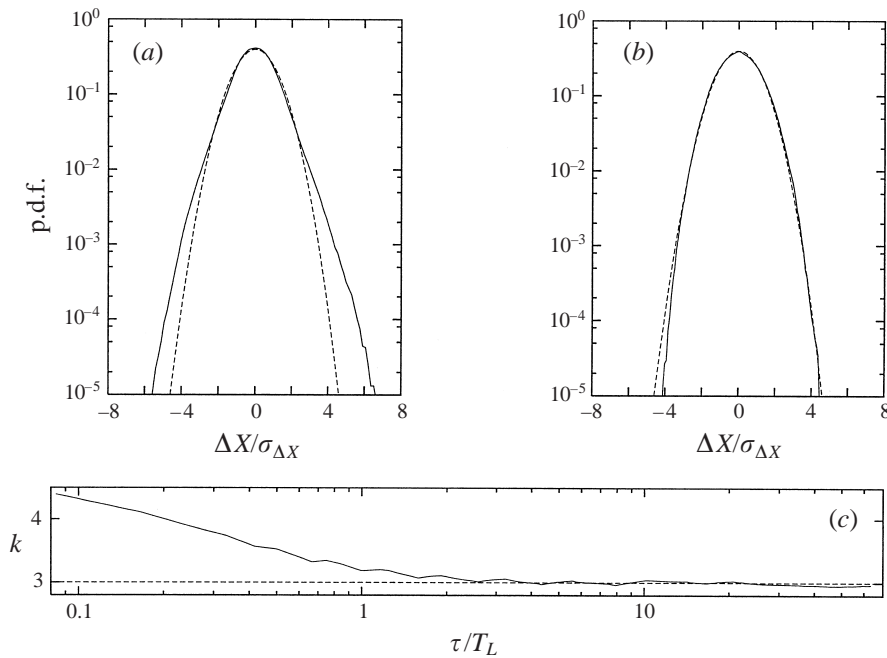


FIGURE 6. Normalized distributions of the displacements  $\Delta X/\sigma_{\Delta X}$  (solid line) at time  $\tau = 0.1T_L$  (a) and  $\tau = 2T_L$  (b). The dashed line represents a Gaussian with the same variance as the observed p.d.f. In (c), the kurtosis of the displacement distribution is plotted as a function of time. After about  $2T_L$ , the kurtosis reaches the value  $k \approx 3$ , indicating that the distribution becomes Gaussian.

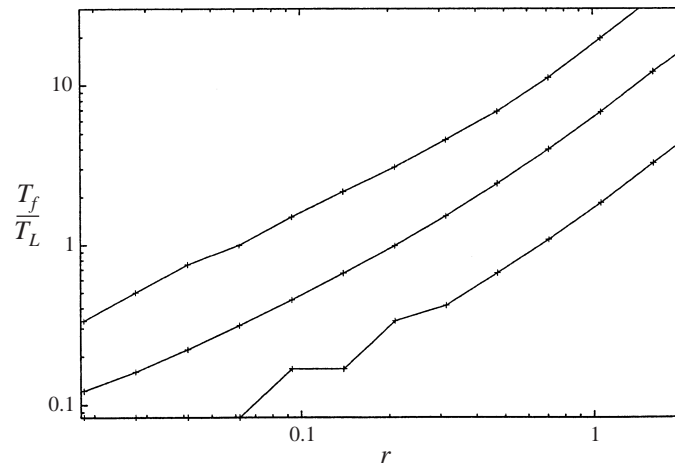


FIGURE 7. First exit time,  $T_f$ , as defined in the text. The middle line is the mean value. The region between the upper and lower curves contains 95% of the data.

#### 4. One-component stochastic models

The aim of a stochastic dispersion model is to reproduce the main statistical properties of particle trajectories in a complex velocity field, without the need for resolving the full dynamics of the Eulerian flow. Stochastic models resort to a description that is characterized by a small number of variables and a simple time evolution.

In this section we compare the outcome of some standard linear and nonlinear stochastic models with the Lagrangian properties of two-dimensional turbulence, as previously determined. As we show in the following, these models do not fully capture the Lagrangian properties of two-dimensional turbulence. In the next section, we introduce a non-Gaussian, two-component model that reproduces more satisfactorily the observed turbulent dispersion properties.

The turbulent velocity field is statistically isotropic, homogeneous, stationary and has zero mean. We assume no statistical correlations between  $U$  and  $V$ , and represent the particle motion as the composite of two one-dimensional stochastic models. In the following, we discuss only the expression for the velocity  $U$  along the  $x$ -direction. The dynamics along the  $y$ -direction are described by an equivalent process.

#### 4.1. Ornstein–Uhlenbeck process

The simplest stochastic model used to represent dispersion with time-correlated increments is based on the Langevin equation for the velocities. The resulting model with Markovian velocities is the Ornstein–Uhlenbeck (OU) process, see e.g. van Dop, Nieuwstadt & Hunt (1985), and Griffa (1996). As these authors observe, this *random flight* model is preferable over the simpler *random walk* model, with Markovian particle positions, whenever the Lagrangian velocities have time correlations. A more sophisticated version of this model can account for correlated accelerations (Sawford 1991; Griffa 1996). In the simulations considered here, however, the Lagrangian accelerations decorrelate on a time scale that is faster than the sampling time  $\delta t$  (which, in turn, is smaller than  $T_Z$ ). Thus, for our purposes, a first-order OU process with correlated velocities suffices.

We write the OU model as

$$\left. \begin{aligned} dX &= U dt, \\ dU &= -\frac{U}{T_L} dt + \sqrt{\frac{2\sigma^2}{T_L}} d\xi, \end{aligned} \right\} \quad (4.1)$$

where  $X(t)$  is the  $x$ -coordinate of a particle,  $U(t)$  is the particle velocity along the  $x$ -axis,  $T_L$  is the velocity decorrelation time,  $\sigma^2 = \langle U^2 \rangle$  is the variance of  $U$ , and  $d\xi(t)$  is a random increment drawn from a normal distribution with zero mean and second-order moment  $\langle d\xi(t) d\xi(t') \rangle = \delta(t - t') dt$  (Wiener process). Initial conditions for the positions  $X(0)$  can be set to zero without loss of generality, and the initial velocity  $U(0)$  is drawn from a Gaussian distribution with zero mean and variance  $\sigma^2$ . Here,  $T_L$  and  $\sigma^2$  are the two free parameters of the model. To compare the OU process with the results obtained from two-dimensional turbulence, we set  $\sigma^2 = 650$  and  $T_L = 0.012$ . In the following, the superscript  $S$  refers to quantities derived from the stochastic model.

For the OU process, the dispersion coefficient can be obtained analytically, as

$$D^S(\tau) = 2\sigma^2 T_L \left[ 1 - \frac{T_L(1 - e^{-\tau/T_L})}{\tau} \right].$$

Note that  $D^S(\tau) \sim \sigma^2 \tau$  for  $\tau \ll T_L$ , and  $D^S(\tau) \sim 2\sigma^2 T_L$  for times  $\tau \gg T_L$ , where the motion is Brownian. The factor of 2 in the expression for  $D(\tau)$  comes from the fact that dispersion is defined for the (vectorial) particle displacement, while  $\sigma^2$  has been defined as the variance of each velocity component. The variance of the vector velocity,  $U = (U, V)$ , is then  $2\sigma^2$ . Figure 8(a) shows the ratio  $D^S/D$  where  $D$  is the

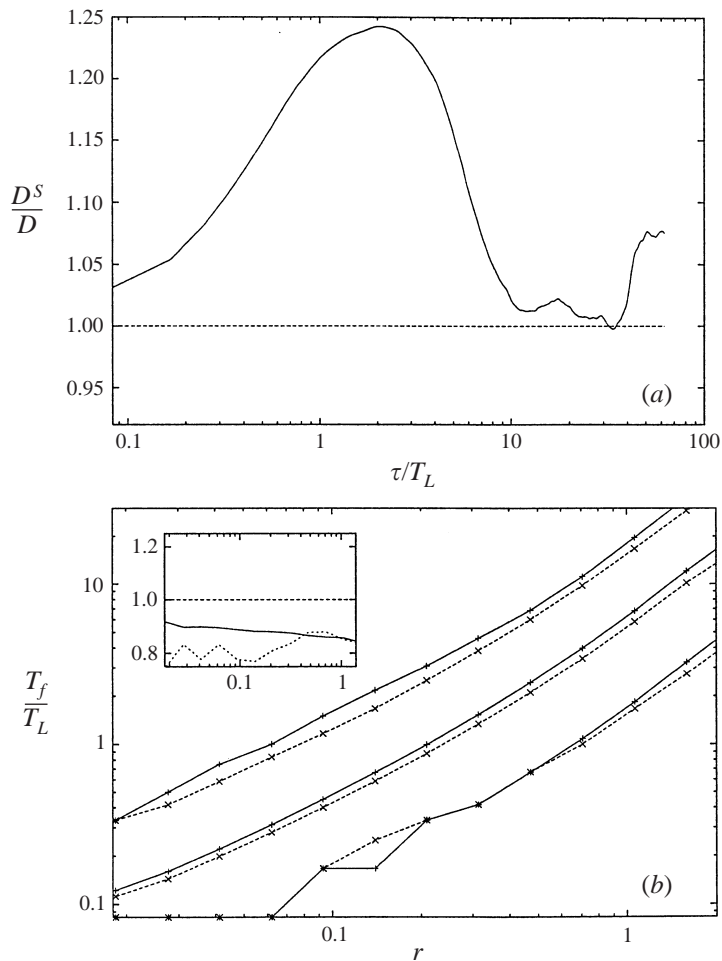


FIGURE 8. (a) Ratio between the dispersion coefficient  $D^S$  from the OU model (4.1) and the dispersion coefficient  $D$  from the turbulent simulation. (b) First exit time, as in figure 7, for the turbulent field (solid lines) and for the OU model (4.1) (dashed lines). The central curves indicate the mean first exit times, while the upper and lower curves bracket 95% of the values of the first exit times as computed from the ensemble of individual trajectories. In the inset, the solid line indicates the ratio between the mean first exit time from the stochastic model,  $T_f^S$ , and the mean first exit time from the turbulent simulation,  $T_f$ . The dotted line indicates the ratio between the upper curves in the main figure, that measure the width of the distribution of first exit times. The closer to unity these lines in the inset are, the better the agreement between the statistics of the turbulent simulation and those of the stochastic model.

dispersion coefficient obtained from two-dimensional turbulence (previously shown in figure 5).

The two curves  $D$  and  $D^S$  fit quite well both at large and short times, as expected from the fact that  $D$  depends only on  $\sigma^2$  and  $T_L$  in these cases. At intermediate times, however,  $D^S$  is larger than  $D$  by up to 25%, indicating that the OU process does not properly capture the turbulent dynamics for times of order of  $T_L$ . Moreover, we recall that, at small times, the distribution of displacements  $\Delta X$  for two-dimensional turbulence is non-Gaussian (see figure 6) and it significantly differs from the one predicted by the OU model, that is always Gaussian.

In figure 8(b) we show the mean first exit time  $T_f^S$  (middle curve) and the upper and lower limits of the interval that contains 95% of the first exit times, as computed from the ensemble of individual trajectories (upper and lower curves). Those provide an estimate of the width of the distribution of first exit times. Both the mean value and the width of the distribution of  $T_{f,i}(r)$  are underestimated by the OU model. This means that the time needed to cover a given distance is on average larger and it is more spread around its mean value in the turbulent case than in the stochastic model.

To summarize, the dynamics of tracers is reproduced well by the OU model only at times  $\tau \gg T_L$ . On such large times the motion is Brownian and it is entirely described by the two parameters that enter the linear stochastic model, namely the velocity variance  $\sigma^2$  and the decorrelation time  $T_L$ . Conversely, for times  $\tau \lesssim 10T_L$ , the OU process does not capture tracer dynamics in two-dimensional turbulence. In the ballistic regime, the dispersion coefficient  $D^S$  is a good approximation, but the non-Gaussianity of the displacement distribution cannot be described by the OU model. Therefore, higher-order moments of the distribution are not reproduced by the stochastic model. Other choices of  $T_L$  and  $\sigma^2$ , consistent with the observed behaviour at large times, do not lead to better agreement with the turbulence data. In the following, we investigate the reasons for the discrepancies and introduce a better description of the Lagrangian motion.

#### 4.2. Non-Gaussian velocity p.d.f.s

The first important difference between the OU model and two-dimensional turbulence is that the turbulent velocity distribution (figure 3) is definitely non-Gaussian. In § 3.1 we briefly discussed how this behaviour is generated by the far-field induced by the coherent vortices (Jiménez 1996; Min *et al.* 1996; Bracco *et al.* 2000b). Thus, we need a stochastic model that is capable of generating non-Gaussian p.d.f.s. Typically, such a model is nonlinear (Thomson 1987).

To parameterize the observed shape of the velocity p.d.f., we write a general empirical form for this distribution as

$$p(U) = A \exp\left(-\frac{U^2}{\sigma_g^2} \frac{1}{1 + |U|/\sigma_e}\right). \quad (4.2)$$

This particular form has been chosen because it tends towards a Gaussian for small velocities and it converges to an exponential for large velocities.

Beside the normalization constant  $A$  (which is fixed by requiring  $\int_{-\infty}^{\infty} p(U) dU = 1$ ), we have the parameters  $\sigma_g$  and  $\sigma_e$ . Their values can be uniquely determined by imposing the following constraints:

second-order moment,

$$\sigma^2 = \int_{-\infty}^{\infty} U^2 p(U) dU,$$

fourth-order moment,

$$k\sigma^4 = \int_{-\infty}^{\infty} U^4 p(U) dU,$$

where  $k$  is the kurtosis of the velocity distribution in the turbulent case,  $k = \langle U^4 \rangle / \langle U^2 \rangle^2$ . To match with our simulations, parameter values are chosen as  $A = 0.0185$ ,  $\sigma_g = 22.6$ ,  $\sigma_e = 42.6$ , where the kurtosis is  $k = 4.1$ . These values have been obtained by numerically solving the integral equations associated with the constraints given above.

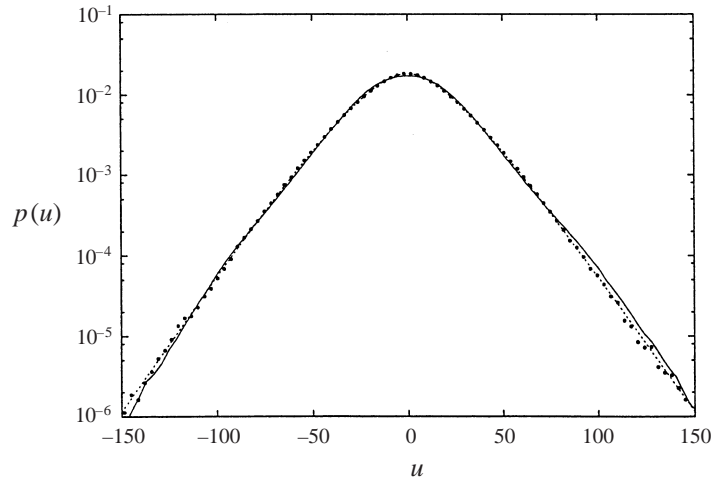


FIGURE 9. Velocity p.d.f. from the Lagrangian trajectories in the turbulent field (solid line) and in the nonlinear stochastic model (4.3), (4.4) (dotted line). The dashed line represents the analytical function  $p(u)$  discussed in the text.

We can then introduce a general form for the stochastic model

$$dX = U dt, \quad dU = a(U) dt + b d\xi, \quad (4.3)$$

with its corresponding Fokker–Planck equation (see e.g. Gardiner 1990)

$$\frac{\partial p(U, t)}{\partial t} = -\frac{\partial}{\partial U} [a p(U, t)] + \frac{1}{2} \frac{\partial^2}{\partial U^2} [b^2 p(U, t)]$$

We next impose that the probability density function is stationary,  $\partial p(U, t)/\partial t = 0$ . By imposing  $b = \text{const}$ , one obtains the form of  $a(U)$  as

$$a(U) = -\frac{b^2}{2\sigma_g^2} \frac{2 + |U|/\sigma_e}{(1 + |U|/\sigma_e)^2} U. \quad (4.4)$$

In the Appendix, we report the details of the calculation that leads to (4.4).

In the simple case considered here, the requirement of stationarity corresponds to the ‘well-mixed condition’ described by Thomson (1987). The latter being fulfilled, convergence to Brownian motion in the limit  $T_L \rightarrow 0$  (or, equivalently,  $t/T_L \rightarrow \infty$ ) is ensured. Thus, the dispersion coefficient  $D$  becomes constant at large times. Given the form of the velocity p.d.f., the saturation value of  $D$  depends on  $b$  only. In the Appendix we show how to obtain the value of  $b$ , from knowledge of the dispersion coefficient.

In figure 9 we show the distribution of Lagrangian velocities generated by the stochastic model (4.3), (4.4). As one can see, this model correctly reproduces the velocity p.d.f. obtained from the turbulent simulation.

In figure 10(a) we show the ratio between the dispersion coefficient obtained from the nonlinear stochastic model (4.3) and that obtained from two-dimensional turbulence. In figure 10(b) we show the first exit time statistics. The distribution of first exit times,  $T_f^S(r)$ , is now closer to the one obtained from the turbulent simulation. The larger spread of this distribution with respect to the OU model is related to the higher probability of having very small and very large velocities, typical of the distribution (4.2). Conversely, no significant improvement in the dispersion coefficient

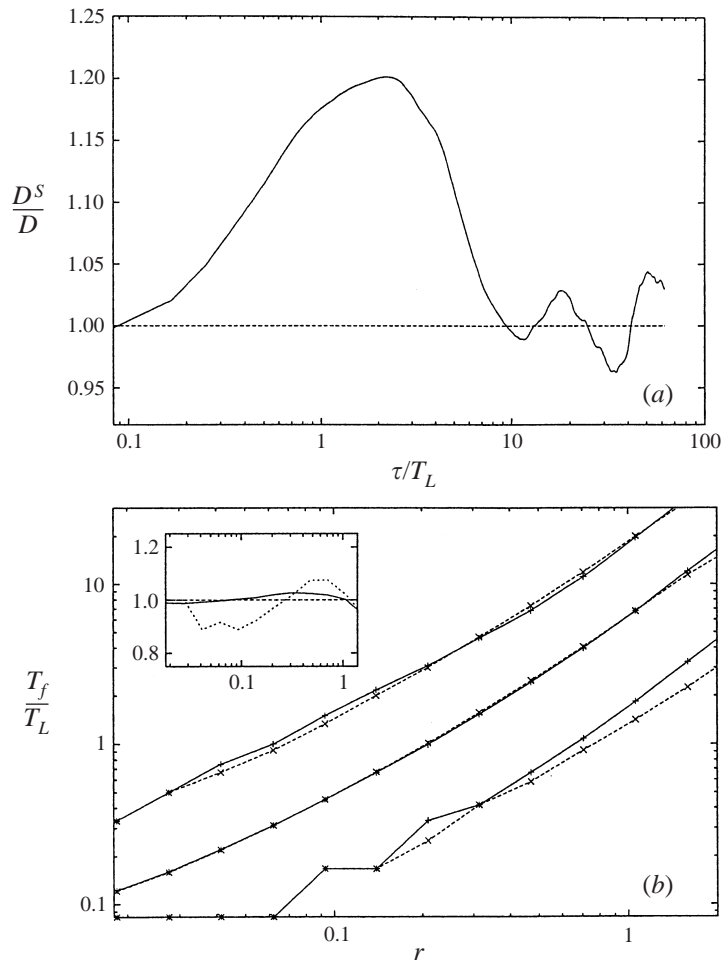


FIGURE 10. Same as figure 8 but for the nonlinear stochastic model (4.3).

is visible. This latter result indicates that the dynamics of tracer dispersion is not fully captured by the nonlinear model (4.3). A different view of the same discrepancy is provided by the comparison between the velocity autocorrelation of the nonlinear stochastic model (4.3) and that of the tracers in the turbulent field. The former is very similar to the exponential decay  $\sim \exp(-\tau/T_L)$  of a OU process, and it is quite different from the turbulent one.

The use of a different analytical shape for the velocity p.d.f. does not lead to better agreement with the observed autocorrelation function. Consider, for instance, a 'bi-Gaussian' description of the velocity distribution, obtained as a weighted sum of two Gaussian distributions with different variance,  $p(U) = A_1 \exp(-U^2/2\sigma_1^2) + A_2 \exp(-U^2/2\sigma_2^2)$ . Such a model is for example used in the study of dispersion in the atmospheric boundary layer (Luhar & Britter 1989; Weil 1990; Maurizi & Tampieri 1999). The corresponding autocorrelation function is shown in figure 11, and it does not provide a better fit to the turbulent autocorrelation. Finally, we also tested whether relaxing the hypothesis of a constant value of the parameter  $b$ , and allowing for a general dependence  $b = b(U)$  and  $a = a(U)$ , could lead to better results. From the

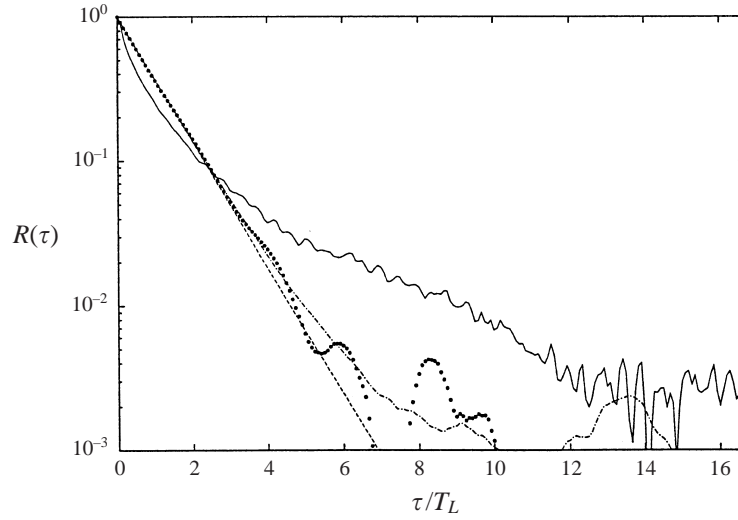


FIGURE 11. Velocity autocorrelation function from tracers in the turbulent field (solid line), for the nonlinear stochastic model (4.3) with the velocity p.d.f. (4.4) (dotted line), and for a bi-Gaussian p.d.f. (dashed-dotted line). The dashed line represents the linear form  $e^{-\tau/T_L}$  as provided by a linear OU process.

second equation of system (4.3), and from  $\langle d\xi \rangle = 0$ , we have

$$\langle dU(U) \rangle = a(U) dt,$$

where the angular brackets indicate an average over all the increments in the velocity interval  $(U, U + dU)$ . We then compute  $a(U) = \langle dU(U) \rangle / dt$  and  $b(U) d\xi = dU(U) - \langle dU(U) \rangle$ . The direct use of these estimates for  $a(U)$  and  $b(U)$  in the stochastic model (4.3) does not lead to significant improvement in the shape of the autocorrelation and in the dispersion coefficient. This suggests that a stochastic model based on a single random process is not sufficient to describe dispersion in two-dimensional turbulence.

For this reason, in the next section we introduce a different model, that is based on physical considerations and reproduces better the observed Lagrangian statistics.

## 5. A two-component stochastic process

Previous explorations of two-dimensional turbulence have shown that this flow can be decomposed into two main constituents, namely the coherent vortices and the background turbulent field (Babiano *et al.* 1987*b*; Bracco *et al.* 2000*b*). Following the idea discussed in Bracco *et al.* (2000*b*), the Eulerian turbulent velocity field is split into two components,  $\mathbf{u}(\mathbf{x}, t) = \mathbf{u}_v(\mathbf{x}, t) + \mathbf{u}_b(\mathbf{x}, t)$ , where  $\mathbf{u}_v$  is generated by the coherent vortices, and  $\mathbf{u}_b$  is generated by the vorticity field outside the vortices (i.e. the background).

To separate the two components, we define a vorticity field,  $\omega_v$ , which is zero outside coherent structures and it is equal to the original field,  $\omega$ , inside them. Analogously, we define the field  $\omega_b$  that is zero inside the vortices and it is equal to the original vorticity field in the background. We then define the velocity field  $\mathbf{u}_v = (u_v, v_v)$  as determined by  $\omega_v$ :

$$u_v(\mathbf{x}) = -\frac{\partial \psi_v}{\partial y} = \frac{i}{\sqrt{2\pi}} \int \frac{k_y}{k^2} \hat{\omega}_v(\mathbf{k}) e^{i\mathbf{k} \cdot \mathbf{x}} d\mathbf{k}$$

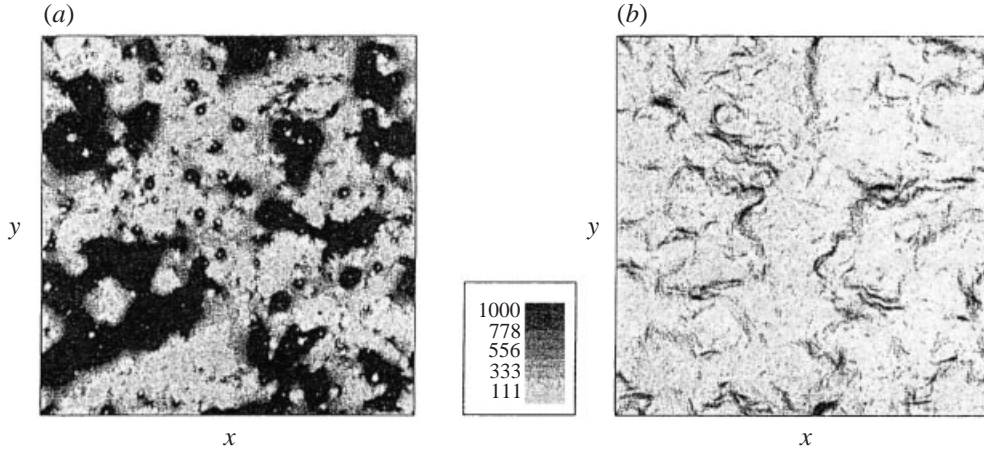


FIGURE 12. Kinetic energy fields associated with the two dynamical components of the vorticity field shown in figure 1. Darker regions indicate higher energy. (a) The energy of the vortex-induced velocity field, and (b) the energy of the background-induced velocity field.

and

$$v_v(\mathbf{x}) = \frac{\partial \psi_v}{\partial x} = \frac{-i}{\sqrt{2\pi}} \int \frac{k_x}{k^2} \hat{\omega}_v(\mathbf{k}) e^{i\mathbf{k}\cdot\mathbf{x}} d\mathbf{k}$$

where  $\psi_v$  is the stream function,  $\hat{\omega}_v$  is the Fourier transform of the field  $\omega_v$ , and  $\mathbf{k} = (k_x, k_y)$  is the wavenumber. The velocity field  $\mathbf{u}_b$  is similarly obtained from the vorticity field  $\omega_b$ . From these definitions, the total field  $\mathbf{u}$  is given by the sum of the two components,  $\mathbf{u}_v$  and  $\mathbf{u}_b$ . Note that the two fields  $\omega_v$  and  $\omega_b$  are ‘local’ and well-separated, i.e. where one of them is non-zero then the other vanishes. However, the two fields  $\mathbf{u}_v$  and  $\mathbf{u}_b$  are non-local, and, particularly outside the vortices, both  $\mathbf{u}_v$  and  $\mathbf{u}_b$  contribute to the total velocity field  $\mathbf{u}$ .

To build a two-component stochastic model in practice, we separate the vortices from the background and define the vorticity fields  $\omega_v$  and  $\omega_b$ . To this end, we use an approximate criterion based on the value of the Okubo–Weiss parameter,  $Q = S^2 - \omega^2$ , where  $\omega^2$  is the square of the vorticity and  $S^2 = S_n^2 + S_s^2$  is the total squared strain (Okubo 1970; Weiss 1991). Here  $S_n = \partial_x u - \partial_y v$  is the normal component of strain and  $S_s = \partial_y u + \partial_x v$  is the shear component. The cores of the coherent vortices are characterized by  $Q \ll 0$  (i.e. rotation dominates), while the background is characterized by  $Q \approx 0$  (i.e. vorticity and strain are in approximate balance). Around the vortices, there is a region where  $Q$  is definitely positive and the flow is strain-dominated (e.g. Elhmaidi *et al.* 1993). Thus, in the following we use the value of  $Q$  to separate the vortex cores from the rest of the turbulent flow. In particular, we define the field  $\omega_v$  as given by the contribution of all those regions for which  $Q < \tilde{Q} = -0.2\sigma_Q$ , where  $\sigma_Q$  is the root-mean-square fluctuation of  $Q$  in the whole field. In turn,  $\omega_b$  comes from all the regions for which  $Q \geq \tilde{Q}$ . (Note, however, that the particular scheme used for the identification of coherent vortex cores does not qualitatively affect the picture described here, see e.g. Bracco *et al.* 2000b. In particular, a vortex-identification scheme based on a simple vorticity threshold provides equivalent results.)

Knowing  $\omega_v$  and  $\omega_b$ , we calculate the two velocity fields  $\mathbf{u}_v$  and  $\mathbf{u}_b$  as discussed above. Figure 12 shows the kinetic energy fields associated with the vortex-induced velocity,  $E_v = \frac{1}{2} \int dx dy \mathbf{u}_v^2$  (part a), and with the background-induced velocity,  $E_b =$



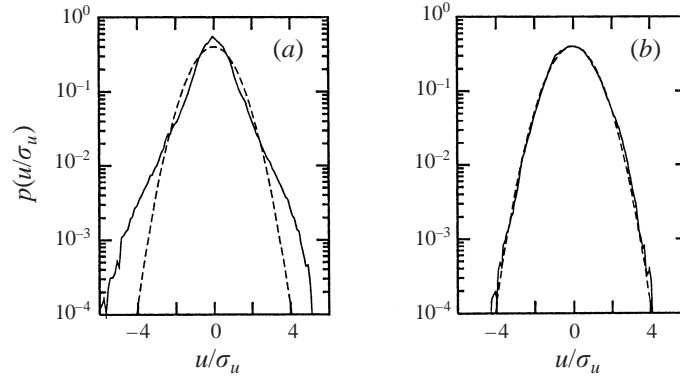


FIGURE 13. Velocity p.d.f.s of the normalized velocity fields  $\mathbf{u}_v$  and  $\mathbf{u}_b$ , whose energy is shown in figure 12. (a) The vortex-induced component and (b) the background-induced component. The two velocity distributions have been normalized to their specific root-mean-square values, and the dashed lines represent a Gaussian distribution.

$\frac{1}{2} \int dx dy \mathbf{u}_b^2$  (part b), for the snapshot corresponding to the vorticity field shown in figure 1. Dark tones correspond to high energy while light tones correspond to low energy. Note that the total energy of the turbulent field can be written as  $E = E_v + E_b + E_i$ , where  $E_i = \int dx dy \mathbf{u}_v \cdot \mathbf{u}_b$  is the covariance of the two velocity components  $\mathbf{u}_v$  and  $\mathbf{u}_b$ , and  $E_i/E$  represents the correlation between the two fields. The value of  $E_i$  is about 10% of the total energy, and it is not represented in figure 12. The energy associated with the velocity field induced by the vortices is the largest, and it is about 8–9 times the energy associated with the velocity field induced by the background. The effect of the background vorticity consists in adding a low-energy unstructured velocity field to the high-energy structured field generated by the vortices.

In figure 13 we show the p.d.f.s of the two velocity components, each normalized to its root-mean-square value. From this figure, one clearly sees that the non-Gaussian velocity p.d.f.s are generated by the vortices. The field  $\mathbf{u}_b$  has a Gaussian distribution, suggesting that it can be described by a linear, Gaussian stochastic process. (On the Gaussianity of the field  $\mathbf{u}_b$  see also Farge, Schneider & Kevlahan 1999.)

To further characterize the dynamics of the two components,  $\mathbf{u}_v$  and  $\mathbf{u}_b$ , we associate a mean eddy turnover time with each of these fields, providing an estimate of the relevant time scales for the two components. Since enstrophy is quite different inside and outside coherent structures, we expect these two time scales to differ significantly. We calculate the background eddy turnover time as  $T_{Zb} = Z_b^{-1/2}$ , where  $Z_b$  is the mean enstrophy outside vortices, and the vortex eddy turnover time as  $T_{Zv} = Z_v^{-1/2}$ , where  $Z_v$  is the mean enstrophy inside vortices. This gives  $T_{Zb} = 0.042 \pm 0.005$  and  $T_{Zv} = 0.009 \pm 0.003$ . The error bars have been obtained by varying the vortex identification threshold,  $\tilde{Q}$ , by a factor of 10, namely from  $\tilde{Q} = -0.1\sigma_Q$  to  $\tilde{Q} = -\sigma_Q$ . Different identification schemes have also been used (such as a simple vorticity threshold) and the corresponding eddy turnover times fall within the error bars given above.

We now use the above information to introduce a new stochastic model that accounts for the presence of two dynamical components,  $\mathbf{U}_v$  and  $\mathbf{U}_b$ , respectively associated with the vortex-induced dynamics and with the background-induced motion. To the sake of simplicity, we make the assumption that  $\mathbf{U}_v$  and  $\mathbf{U}_b$  are independent

of each other. This approximation is suggested by the fact that the large vorticity gradients at the edge of the vortices inhibit vorticity exchanges between the vortex cores and the surrounding turbulence, as well as by the fact that the vorticity level of the background is too low to significantly influence the dynamics of the vortices, once they have formed. Note, however, that vortex–vortex interactions have a significant impact on the turbulent background, due, for example, to the ejection of filaments with high vorticity. On the other hand, explicit consideration of the vortex–background interaction could considerably complicate the picture, and thus we opted for discarding it here. We were encouraged in this decision by the fact that the correlation between  $\mathbf{u}_v$  and  $\mathbf{u}_b$ ,  $E_i/E$ , is of order 0.1. Note, however, that  $E_i \sim E_b$ , and a more refined model should take into account the role of filaments ejected during vortex interactions. Thus, the model introduced here should be considered only as a first approximation.

In the following, we thus simply consider two independent stochastic processes separately describing the two types of velocity,  $U_v$  and  $U_b$ , and we sum them to obtain the total velocity of the advected particles,  $U = U_v + U_b$ . We call  $\sigma_v^2$ ,  $T_{Lv}$  and  $\sigma_b^2$ ,  $T_{Lb}$  the variance and the decorrelation time of the two components respectively. Owing to the independence of  $U_v$  and  $U_b$ , the general form of the autocorrelation function for the total velocity  $U$  becomes

$$\begin{aligned} R(\tau) &= \frac{\langle (U_v(t) + U_b(t)) \cdot (U_v(t + \tau) + U_b(t + \tau)) \rangle}{\sigma^2} \\ &= \frac{\langle (U_v(t)) \cdot (U_v(t + \tau)) \rangle}{\sigma^2} + \frac{\langle (U_b(t)) \cdot (U_b(t + \tau)) \rangle}{\sigma^2} \\ &= \frac{\sigma_v^2}{\sigma^2} R_v(\tau) + \frac{\sigma_b^2}{\sigma^2} R_b(\tau), \end{aligned}$$

where  $R_v(\tau)$  and  $R_b(\tau)$  are the Lagrangian autocorrelation functions of  $U_v$  and  $U_b$  respectively.

As a first step, we suppose that the components  $U_v$  and  $U_b$  are described by two different linear Gaussian stochastic processes. The total two-component process is thus given by

$$\left. \begin{aligned} dX &= (U_v + U_b) dt, \\ dU_v &= -\frac{1}{T_{Lv}} U_v dt + \sqrt{\frac{2\sigma_v^2}{T_{Lv}}} d\xi_v, \\ dU_b &= -\frac{1}{T_{Lb}} U_b dt + \sqrt{\frac{2\sigma_b^2}{T_{Lb}}} d\xi_b. \end{aligned} \right\} \quad (5.1)$$

In this system we have to determine four parameters, namely  $\sigma_v$ ,  $\sigma_b$ ,  $T_{Lv}$ , and  $T_{Lb}$ , which are related to each other by the following constraints:

value of the total variance,  $\sigma^2 = \sigma_v^2 + \sigma_b^2$ ;

value of the total integral Lagrangian time,  $T_L = (\sigma_v^2/\sigma^2)T_{Lv} + (\sigma_b^2/\sigma^2)T_{Lb}$ .

The empirical determination of two other parameters, in addition to  $\sigma^2$  and  $T_L$  that have already been determined, is thus required to fully define the model. To this end, we note that the process that decorrelates more rapidly does not significantly affect the autocorrelation function at large times, and thus the long-time form of the autocorrelation is approximately determined by just one of the two processes. Thus, we opt for the evaluation of the parameters related to the slowest and less energetic process, obtained by fitting the autocorrelation curve at large times.

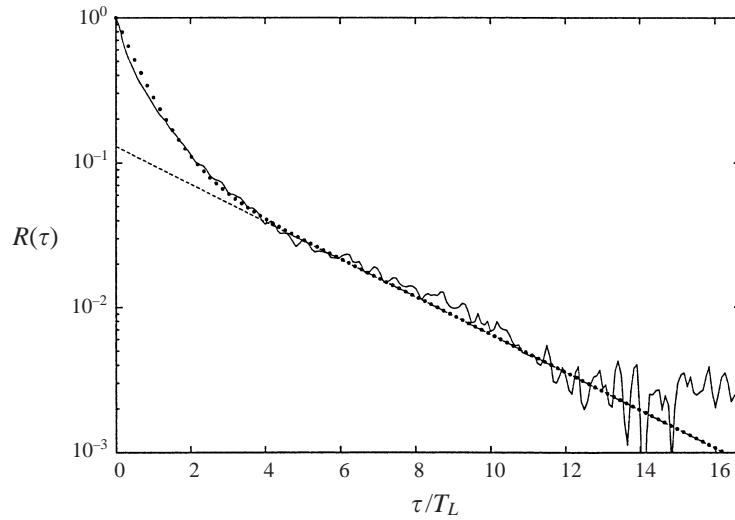


FIGURE 14. Velocity autocorrelation function from tracers in the turbulent field (solid line) and for the two-components stochastic model (dotted line). The dashed line represents the fit to the autocorrelation function at large times; its intersection with the vertical axis gives  $\sigma_b^2/\sigma^2$  (see text).

The fact that the eddy turnover time for the background,  $T_{Zb}$ , is larger than that for the vortices,  $T_{Zv}$ , suggests associating the largest Lagrangian decorrelation time with the background-induced motion. The decorrelation time  $T_{Lb}$  is approximated by the semilogarithmic slope of  $R(\tau)$  at large times (see figure 14), while the variance  $\sigma_b^2$  can be obtained by intersecting the extrapolation of the fitting line with the vertical axis at  $\tau = 0$ . The value of the intersection is the ratio  $\sigma_b^2/\sigma^2$ . Clearly, this approach works only if the two decorrelation times are sufficiently different from each other. In the present case,  $T_{Lv}$  and  $T_{Lb}$  differ by a factor of five, and the whole procedure can be successfully applied.

In the following, we thus perform a least-square fit to the logarithm of the velocity autocorrelation function to calculate  $T_{Lb}$  and  $\sigma_b^2$ . The maximum time  $\tau$  for defining the fitting range is chosen as  $13T_L$ , since after this time the autocorrelation displays strong fluctuations. The minimum time for the fitting range is determined by the time lag after which the correlation due to the vortex-induced component of the velocity vanishes. We vary this value in the range  $2.5T_L$  to  $5T_L$ . In this way, the parameter values that we obtain are  $T_{Lb} = 0.040 \pm 0.001$  and  $\sigma_b^2 = 85 \pm 5$ . From the constraints discussed above, we obtain  $T_{Lv} = 0.0070 \pm 0.0005$  and  $\sigma_v^2 = 565 \pm 5$ . Note, in particular, that the decorrelation times for the background component,  $T_{Lb}$ , and for the vortex component,  $T_{Lv}$ , are in close agreement with the mean eddy turnover times determined from the Eulerian analysis. This provides confidence in the whole procedure of considering a two-component description of the advecting turbulent velocity.

With this choice of the component processes, the distribution function of the total velocity ( $U_v + U_b$ ) is still Gaussian, with variance  $\sigma^2 = \sigma_v^2 + \sigma_b^2$ . The dispersion obtained with the two-components model is shown in figure 15(a). The improvement with respect to the other stochastic processes is clearly visible. The first exit time statistics, however, are very similar to those given by the standard OU model (see figure 15b), since they are related to the higher-order moments of the velocity distribution, which are not captured by a linear model.

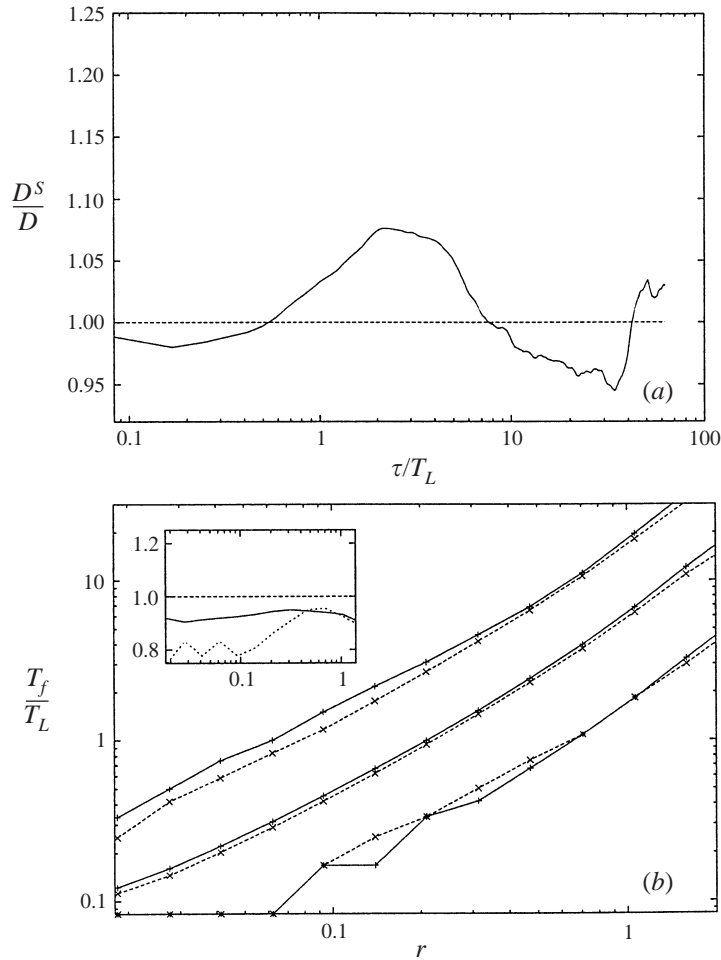


FIGURE 15. Same as figure 8 but for the two-components stochastic model (5.1).

To correct this problem, we reintroduce the non-Gaussianity in the vortex-induced velocity p.d.f. As previously described, the vortex-induced component  $U_v$  has a non-Gaussian distribution, while  $U_b$  is Gaussian and can be represented by a linear OU model. The appropriate stochastic model for the description of both the non-Gaussian velocity p.d.f. and the non-exponential autocorrelation function can thus be cast in the form

$$\left. \begin{aligned} dX &= (U_v + U_b) dt, \\ dU_v &= a(U_v) dt + b d\xi_v, \\ dU_b &= -\frac{1}{T_{Lb}} U_b dt + \sqrt{\frac{2\sigma_b^2}{T_{Lb}}} d\xi_b. \end{aligned} \right\} \quad (5.2)$$

with  $a(U_v)$  given by equation (4.4). This model has five parameters, namely (a) the variance and the decorrelation time of the vortex-induced velocity, (b) the variance and the decorrelation time of the background-induced velocity, and (c) the fourth-

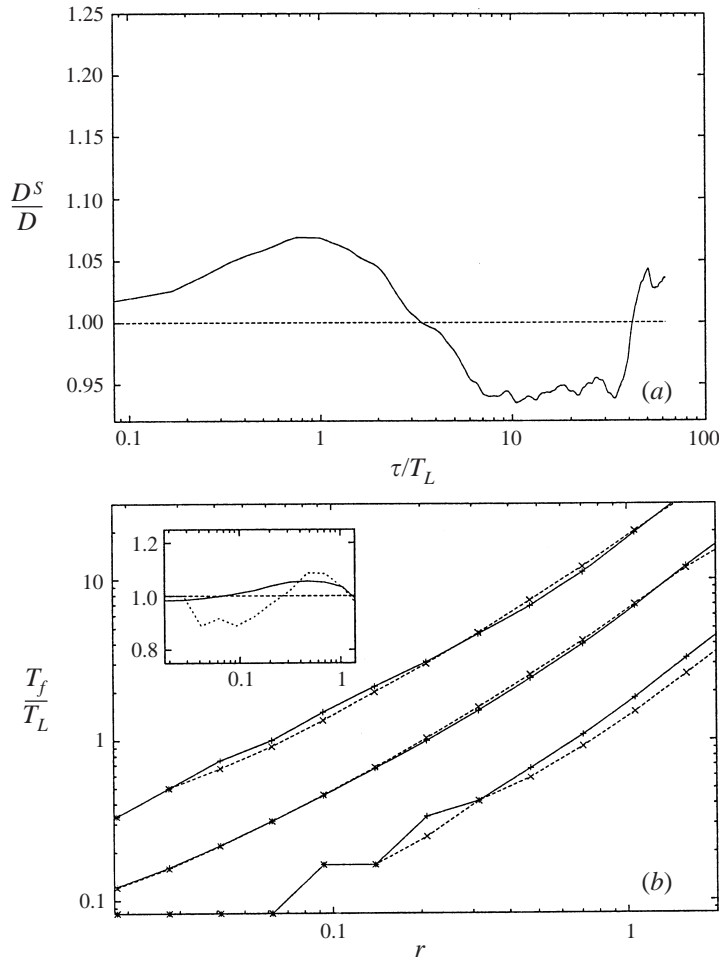


FIGURE 16. Same as figure 8 but for the stochastic model (5.2).

order moment of the vortex-induced velocity distribution. The values of the parameters for the background component have been previously determined,  $\sigma_b^2 = 85 \pm 5$  and  $T_{Lb} = 0.04 \pm 0.001$ . For the vortex-induced velocity component, we impose the second-order moment of the velocity distribution to be  $\sigma_v^2 = 565$ , such that  $\sigma_v^2 + \sigma_b^2 = \sigma^2$ , and the kurtosis to be  $k_v \simeq 4.1$ , such that the total velocity distribution in the model has the same kurtosis as the turbulent velocity distribution. A numerical integration of the above constraints leads to  $\sigma_g = 12.1 \pm 0.2$  and  $\sigma_e = 7.60 \pm 0.02$ . Finally, the value of  $b = 420$  is chosen as described in the Appendix, based on the requirement that the integral Lagrangian time is  $T_{Lv} = 0.007$ , as previously obtained. As can be seen in figure 16, with this model both the dispersion coefficient and the first exit times are reproduced well. The introduction of the nonlinearity is necessary to reproduce the non-Gaussian velocity distribution and it allows correct first exit time statistics to be obtained. On the other hand, the consideration of two velocity components with different decorrelation times is necessary for a proper description of the dispersion at intermediate times.

## 6. Discussion and conclusions

Rotating turbulent flows, such as the ocean and the atmosphere, are characterized by the presence of long-lived coherent vortices (see e.g. Bengtson & Lighthill 1982; Hopfinger & van Heijst 1993; Ring Group 1981). They also extend their influence to the far field, and induce non-Gaussian velocity distributions in the background turbulence (Bracco *et al.* 2000*a,b*). The turbulent dynamics between the vortices is simultaneously affected by both the far field of the vortices and the local background vorticity field, leading to a non-exponential shape of the velocity autocorrelation.

In such a situation, one may wonder whether standard stochastic models devised to parameterize turbulent dispersion (see e.g. Rodean 1996) can provide useful results. In this work we have studied particle advection in two-dimensional turbulence, and we have analysed the performance of different types of stochastic parameterizations of dispersion. Whenever the coherent vortices are smooth and not very intense, as for low Reynolds numbers and/or large-scale forcing, the velocity field can be satisfactorily modelled in terms of a Gaussian red noise (Ornstein–Uhlenbeck process). At larger Reynolds numbers, however, strong coherent structures dominate the dynamics and a simple linear ‘random flight’ model based on the OU process gives an estimate of single-particle dispersion that differs from the true one by at most 25%. In addition, such a linear model does not provide good results for the distribution of minimum exit times, which are in fact determined by the higher-order moments of the velocity distribution. When only the second-order moments are of interest, and uncertainties of about 25% are acceptable (due for example to data errors or imprecise knowledge of the parameters), then such a simple model suffices.

Slightly better results are obtained with a model that explicitly takes into account the non-Gaussian nature of the velocity p.d.f.s. Such a nonlinear stochastic process provides a better description of the minimum exit time statistics, but does not lead to better agreement with the observed single-particle dispersion curve.

The minimal model that satisfactorily reproduces the observed dispersion statistics is based on exploiting the fundamental two-component nature of rotating turbulent flows, which are made up of both a highly coherent set of individual vortices and a low-energy turbulent background field. This latter has a longer decorrelation time, and it dominates the dispersion statistics at late times. Based on these considerations, in this work we have introduced and tested a new stochastic model for parameterizing particle dispersion in two-dimensional turbulence. This model takes into account both the non-Gaussianity of the vortex-induced velocity field and the non-exponential shape of the velocity autocorrelation. The model is based on assuming the existence of two different stochastic processes, related respectively to the vortex dynamics and to the background turbulence. In the limit of large times, the model correctly reduces to Brownian motion. At shorter time scales, the model proposed here satisfactorily reproduces both the single-particle dispersion curve and the distribution of first exit times, providing a significant improvement with respect to both linear and nonlinear single-component models.

The two-component model introduced here has five parameters that can be estimated from the analysis of sample Lagrangian trajectories (such as ocean float data) and does not require knowledge of the Eulerian velocity field. The parameters have been introduced based on physical reasoning, and each of them is related to a well-defined property of the turbulent flow, namely (*a*) the energy and the decorrelation time of the vortex-induced dynamics, (*b*) the energy and the decorrelation time of the background turbulence, and (*c*) a measure of the deviation from Gaussianity of the velocity field determined by the presence of the vortices (e.g. the kurtosis). The

estimate of the parameters is straightforward whenever the two component processes are well separated in their temporal time scale and energy. Given that most of the energy is associated with the coherent structures and that the vortex rotation velocity is much larger than the random fluctuations of the background velocity, the requirement of scale separation is fulfilled by most vortex-dominated flows.

Last, we mention that in the situation considered here the acceleration time scale is much smaller than the sampling time. In other conditions, however, the acceleration time scale can be comparable with the other time scales of the problem (see e.g. Hua, McWilliams & Klein 1998). In such a situation, a second-order model with correlated accelerations should be introduced.

We thank Joe Keller, Annalisa Griffa, Annalisa Bracco, Alberto Maurizi, Francesco Tampieri and Ed Spiegel for useful discussions, and the referees for helping us to improve the manuscript.

## Appendix

We derive the stochastic differential equation that allows a velocity distribution to be obtained of the form

$$p(U) = A \exp\left(-\frac{U^2}{\sigma_g^2} \frac{1}{1 + |U|/\sigma_e}\right).$$

To this end, in the generic stochastic process

$$dX = U dt, \quad dU = a(U) dt + b(U) d\xi \quad (\text{A } 1)$$

we seek the expressions for  $a(U)$  and  $b(U)$  such that the velocity probability density function is  $p(U)$ .

In the Fokker–Planck equation for the stochastic process (A 1), we impose that all derivatives vanish,  $\partial/\partial x = \partial/\partial y = \partial/\partial t = 0$ , consistent with the assumption of homogeneity and stationarity.

From the Fokker–Planck equation we have

$$a(U) p(U) = \frac{d}{dU} \left( \frac{b(U)^2}{2} p(U) \right) + \phi \quad (\text{A } 2)$$

where  $\phi$  is a constant. The value of  $\phi$  is determined by requiring  $\lim_{|U| \rightarrow \infty} \phi = 0$ , which leads to  $\phi = 0$ , so that the integral of expression (A 2) over  $U$ -space exists. Next, we assume that the dissipation rate is not correlated with the velocity, and impose  $db/dU = 0$ . For a discussion of this issue see Thomson (1987). The condition then implies

$$a(U) = \frac{b^2}{2} \frac{1}{p(U)} \frac{dp}{dU}$$

which leads to

$$a(U) = -\frac{b^2}{2\sigma_g^2} \frac{2 + |U|/\sigma_e}{(1 + |U|/\sigma_e)^2} U.$$

The steady-state condition described here is a particular case of the more general ‘well-mixed condition’ introduced by Thomson (1987), that is applicable to non-stationary solutions. Thomson also showed that if the condition is fulfilled, the dispersion coefficient  $D(\tau)$  becomes constant at large times,  $\lim_{\tau \rightarrow \infty} D(\tau) = 2K$ , with a

saturation value given by

$$K = \int_{-\infty}^{\infty} \frac{2q(U)^2}{b^2 p(U)} dU$$

where

$$q(U) = \int_{-\infty}^U V p(V) dV.$$

From the above arguments, it follows that

$$b^2 = \frac{2}{K} \int_{-\infty}^{\infty} \frac{q(U)^2}{p(U)} dU \quad (\text{A } 3)$$

Given the velocity p.d.f. and the large-time limit of the dispersion coefficient, the numerical computation of integral (A 3) leads to the evaluation of the parameter  $b$  for any distribution function.

#### REFERENCES

- BABIANO, A., BASDEVANT, C., LEGRAS, B. & SADOURNY, R. 1987*a* Vorticity and passive-scalar dynamics in two-dimensional turbulence. *J. Fluid Mech.* **197**, 241–257.
- BABIANO, A., BASDEVANT, C., LEROY, P. & SADOURNY, R. 1987*b* Single-particle dispersion, Lagrangian structure function and Lagrangian energy spectrum in two-dimensional incompressible turbulence. *J. Mar. Res.* **45**, 107–131.
- BABIANO, A., BOFFETTA, G., PROVENZALE, A. & VULPIANI, A. 1994 Chaotic advection in point vortex models and two-dimensional turbulence. *Phys. Fluids* **6**, 2465–2474.
- BASDEVANT, C. & SADOURNY, R. 1983 Simulation numérique des écoulements turbulents bi-dimensionnels. *J. Méc. Théor. Appl.* Numéro Spécial, 243–269.
- BENGTSON, L. & LIDTHILL, J. (Eds.) 1982 *Intense Atmospheric Vortices*. Springer.
- BRACCO, A., LACASCE, J. & PROVENZALE, A. 2000*a* Velocity pdf's for oceanic floats. *J. Phys. Oceanogr.* **30**, 461–474.
- BRACCO, A., LACASCE, J., PASQUERO, C. & PROVENZALE, A. 2000*b* The velocity distribution of barotropic turbulence. *Phys. Fluids* **12**, 2478–2488.
- DOP, H. VAN, NIEUWSTADT, F. T. M. & HUNT, J. C. R. 1985 Random walk models for particle displacements in inhomogeneous unsteady turbulent flows. *Phys. Fluids* **28**, 1639–1653.
- ELHMAIDI, D., PROVENZALE, A. & BABIANO, A. 1993 Elementary topology of two-dimensional turbulence from a Lagrangian viewpoint and single-particle dispersion. *J. Fluid Mech.* **242**, 655–700.
- FARGE, M., SCHNEIDER, K. & KEVLAHAN, N. 1999 Non-Gaussianity and coherent vortex simulation for two-dimensional turbulence using an adaptive orthogonal wavelet basis. *Phys. Fluids* **11**, 2187–2201.
- FIGUEROA, H. A. & OLSON, D. B. 1994 Eddy resolution versus eddy diffusion in a double gyre GCM. Part I: The Lagrangian and Eulerian description. *J. Phys. Oceanogr.* **24**, 371–402.
- GARDINER, C. W. 1990 *Handbook of Stochastic Methods*. Springer.
- GIFFORD, F. A. 1982 Horizontal diffusion in the atmosphere: A Lagrangian-dynamical theory. *Atmos. Environ.* **16**, 505–512.
- GRIFFA, A. 1996 Applications of stochastic particle models to oceanographic problems. In *Stochastic Modelling in Physical Oceanography* (ed. R. J. Adler, P. Müller & R. B. Rozovskii), pp. 114–140. Birkhäuser.
- HARDENBERG, J. VON, FRAEDRICH, K., LUNKEIT, F. & PROVENZALE, A. 2000 Transient chaotic mixing during a baroclinic life cycle. *Chaos* **10**, 122–134.
- HOPFINGER, E. J. & HEIJST, G. J. F. VAN 1993 Vortices in rotating fluids. *Ann. Rev. Fluid Mech.* **25**, 241–289.
- HALLER, G. & YUAN, G. 2000 Lagrangian coherent structures and mixing in two-dimensional turbulence. *Physica D* **147**, 352–370.
- HUA, B. L., MCWILLIAMS, J. C. & KLEIN, P. 1998 Lagrangian accelerations in geostrophic turbulence. *J. Fluid Mech.* **366**, 87–108.



- JIMÉNEZ, J. 1996 Algebraic probability density tails in decaying isotropic two-dimensional turbulence. *J. Fluid Mech.* **313**, 223–240.
- LEGRAS, B., SANTANGELO, P. & BENZI, R. 1988 High-resolution numerical experiments for forced two-dimensional turbulence. *Europhys. Lett.* **5**, 37–42.
- LUHAR, A. K. & BRITTER, R. E. 1989 A random walk model for diffusion in inhomogeneous turbulence in a convective boundary layer. *Atmos. Environ.* **23**, 1911–1924.
- MAURIZI, A. & TAMPIERI, F. 1999 Velocity probability density functions in Lagrangian dispersion models for inhomogeneous turbulence. *Atmos. Environ.* **33**, 281–289.
- MAXEY, M. R. & RILEY, J. J. 1983 Equation of motion for a small rigid sphere in a nonuniform flow. *Phys. Fluids* **26**, 883–889.
- MICHAELIDES, E. E. 1997 The transient equation of motion for particles, bubbles, and droplets. *Trans. ASME: J. Fluids Engng* **119**, 233–247.
- MIN, I. A., MEZIC, I. & A. LEONARD, A. 1996 Levy stable distributions for velocity and velocity difference in systems of vortex elements. *Phys. Fluids* **8**, 1169–1180.
- MCWILLIAMS, J. C. 1984 The emergence of isolated coherent vortices in turbulent flow. *J. Fluid Mech.* **146**, 21–43.
- OKUBO, A. 1970 Horizontal dispersion of floatable particles in the vicinity of velocity singularities such as convergences. *Deep-Sea Res.* **17**, 445–454.
- PEDLOSKY, J. 1987 *Geophysical Fluid Dynamics*. Springer.
- PIERREHUMBERT, R. T. 1991 Chaotic mixing of tracer and vorticity by modulated travelling Rossby waves. *Geophys. Astrophys. Fluid Dyn.* **58**, 285–319.
- PIERREHUMBERT, R. T. & YANG, H. 1993 Global chaotic mixing on isentropic surfaces. *J. Atmos. Sci.* **50**, 2462–2480.
- POJE, A. & HALLER, G. 1999 Geometry of cross-stream mixing in a double-gyre ocean model. *J. Phys. Oceanogr.* **29**, 1649–1665.
- PROVENZALE, A. 1999 Transport by coherent vortices. *Ann. Rev. Fluid Mech.* **31**, 55–93.
- PROVENZALE, A., BABIANO, A. & VILLONE, B. 1995 Single-particle trajectories in two-dimensional turbulence. *Chaos, Solitons and Fractals* **5**, 2055–2071.
- RING GROUP 1981 Gulf stream cold core ring: their physics, chemistry and biology. *Science* **212**, 1091–1100.
- RODEAN, H. C. 1996 Stochastic Lagrangian models of turbulent diffusion. *Meteor. Monographs* **26**(48).
- ROGERSON, A. M., MILLER, P. D., PRATT, L. J. & JONES, C. K. R. T. 1999 Lagrangian motion and fluid exchange in a barotropic meandering jet. *J. Phys. Oceanogr.* **29**, 2635–2655.
- SALMON, R. 1998 *Lecture Notes on Geophysical Fluid Dynamics*. Oxford University Press.
- SAMELSON, R. M. 1992 Fluid exchange across a meandering jet. *J. Phys. Oceanogr.* **22**, 431–440.
- SAWFORD, B. L. 1991 Reynolds number effects in Lagrangian stochastic models of turbulent dispersion. *Phys. Fluids A* **3**(6), 1577–1586.
- SAWFORD, B. L. & BORGAS, M. S. 1994 On the continuity of stochastic models for the Lagrangian velocity in turbulence. *Physica D* **76**, 297–311.
- SOLOMON, T. H., WEEKS, E. R. & SWINNEY, H. L. 1993 Observation of anomalous diffusion and Levy flights in a two-dimensional rotating flow. *Phys. Rev. Lett.* **71**, 3975–3978.
- TAYLOR, G. I. 1921 Diffusion by continuous movement. *Proc. Lon. Math. Soc.* **20**, 196–212.
- THOMSON, D. J. 1987 Criteria for the selection of stochastic models of particle trajectories in turbulent flows. *J. Fluid Mech.* **180**, 529–556.
- WEIL, J. C. 1990 A diagnosis of the asymmetry in top-down and bottom-up diffusion using a Lagrangian stochastic model. *J. Atmos. Sci.* **47**, 501–515.
- WEISS, J. B. 1991 The dynamics of enstrophy transfer in two-dimensional hydrodynamics. *Physica D* **48**, 273–294.
- WEISS, J. B. & KNOBLOCH, E. 1987 Mass transport and mixing by modulated traveling waves. *Phys. Rev. A* **40**, 2579–2589.
- WEISS, J. B., PROVENZALE, A. & MCWILLIAMS, J. C. 1998 Lagrangian dynamics in high-dimensional point-vortex systems. *Phys. Fluids* **10**, 1929–1941.
- WIGGINS, S. 1992 *Chaotic Transport in Dynamical Systems*. Springer.